

# Production of defects in supported carbon nanotubes under ion irradiation

A. V. Krasheninnikov, K. Nordlund, and J. Keinonen

*Accelerator Laboratory, P.O. Box 43, FIN-00014 University of Helsinki, Finland*

(December 10, 2001)

Ion irradiation of individual carbon nanotubes deposited on substrates may be used for making metallic nanowires and studying effects of disorder on the electronic transport in low-dimensional systems. In order to understand the basic physical mechanisms of radiation damage production in supported nanotubes, we employ molecular dynamics and simulate ion impacts on nanotubes lying on different substrates, such as platinum and graphite. We show that the defect production depends on the type of the substrate and the damage is higher for metallic heavy-atom substrates than for light-atom substrates, since in the former case sputtered metal atoms and backscattered recoils produce extra damage in the nanotube. We further study the behavior of defects upon high-temperature annealing and demonstrate that, although ions may severely damage nanotubes in a local region, the nanotube carbon network has a unique ability to heal such a strong localized damage due to defect migration and dangling bond saturation. We also show that after annealing the residual damage in nanotubes is independent of the substrate type. We predict pinning of nanotubes to substrates through nanotube-substrate bonds which appear near irradiation-induced defects.

81.07.De, 61.48+c, 61.80.Jh,73.22.-f

## I. INTRODUCTION

Recent theoretical and experimental studies<sup>1-9</sup> on the irradiation of carbon nanotubes with energetic particles have revealed a broad range of new interesting phenomena. These are, e.g., the coalescence<sup>2</sup> and welding<sup>3</sup> of nanotubes under electron irradiation, ion irradiation-induced changes in electrical coupling between nanotubes,<sup>4</sup> surface reconstructions,<sup>5,6</sup> modifications of mechanical properties<sup>7</sup> and a decrease in the contact resistance between a carbon nanotube and metallic electrodes after the contact area has been exposed to a focused electron beam.<sup>8</sup> Experiments also provide evidence that ion irradiation and nanotubes may be employed for fabricating metal nanowires on insulating substrates using carbon nanotubes as masks.<sup>10</sup> By irradiating with 300 eV Ar<sup>+</sup> ions, a Au/Ti wire a few nanometers in width has been formed just underneath a carbon nanotube lying on a thin Au/Ti layer deposited earlier on a SiO<sub>2</sub> substrate.<sup>10</sup>

These examples illustrate the demand for microscopic understanding of defect formation mechanisms in carbon nanotubes under irradiation, and comprehension of the subsequent time evolution of the irradiation-induced defects.

The microscopic behavior of nanotubes under electron irradiation has been investigated at length.<sup>1,2,5,6</sup> Reconstructions of the carbon network and drastic dimensional changes have been reported, as a corollary of which the apparent diameter of nanotubes shrinks from  $\approx 1.4$  to 0.4 nm. Tight-binding and Monte-Carlo simulations<sup>2,5</sup> indicate that the mechanism which gives rise to the dimensional changes and nanotube coalescence is the reorganization of atoms in the nanotube carbon network due to healing irradiation-induced vacancies through dangling bond saturation.

The formation of defects in individual suspended nanotubes by energetic ions has also been studied by means of atomistic simulations.<sup>11</sup> Such individual nanotubes can be experimentally produced by suspending them between metallic electrodes using a self-aligned oxide etching technique.<sup>12</sup> It has been shown that the most prolific defects in nanotubes which appear under ion irradiation are vacancies. At low temperatures they are metastable but macroscopically long-lived defects (at least of the order of hours). This result is in line with the experimental observations of the characteristic times and temperatures under which the coalescence of nanotubes occurs under electron irradiation.<sup>2</sup> Note that ion irradiation makes it possible to create much stronger damage in a local region than that produced by electron irradiation, with the number of displacements per atom and per second being also much larger for the same flux.

The response of nanotubes in bundles to irradiation has been studied as well. The bombardment of a bundle of single-walled nanotubes by CH<sub>3</sub> radicals<sup>9</sup> or with energetic ions<sup>13</sup> gives rise to cross-linking and functionalization of the nanotubes.

However, the mechanism of defect creation in supported nanotubes, i.e., nanotubes on different substrates, has not yet been addressed, although such systems, apart from the fact that they can be used as mask for making nanowires, may be utilized in various key experiments. In particular, those may be scanning tunneling microscopy probing of the irradiated nanotubes<sup>11,14</sup> to locate and characterize irradiation-induced defects or transport studies on quasi-one-dimensional systems with disorder.<sup>15-18</sup> The presence of a substrate may play a dominant role upon irradiating supported nanotubes, since in that case the nanotubes can be damaged by backscattered impinging particles or atoms sputtered from the substrate.

In this work, we study the ion irradiation of single-walled nanotubes on different substrates. We also dwell upon the subsequent time evolution and annealing of the irradiation-induced defects. For obtaining qualitative understanding of the physical processes involved, we considered two limiting cases: a heavy-atom metallic substrate and a light-atom substrate with covalent bonds between atoms. The former was chosen to be the platinum (111) surface, the latter the Bernal graphite (0001) surface. Noble metals<sup>19,20</sup> and graphite<sup>20,21</sup> have repeatedly been used as substrates in experimental studies on carbon nanotubes.

This paper is organized as follows. In the following section, we briefly review the molecular dynamics technique used to study the defect production in nanotubes under ion irradiation. Since this simulation technique is well established, our description will be brief and restricted to issues directly effecting our simulations. Section III presents the results of our study as well as their discussion. A summary of the results is given in section IV.

## II. THE SIMULATION METHOD

We used classical molecular dynamics<sup>22</sup> to model the defect production in nanotubes under argon ion irradiation. This is the only method fast enough both for simulating realistically energetic collisional processes and achieving representative statistics. To model C-C interaction, we used the Brenner II interatomic potential.<sup>23</sup> This potential has been repeatedly used for simulating carbon nanotubes and a good correlation between the results of classical simulations and *ab initio* calculations has been reported.<sup>24,25</sup> Because the bond conjugation is not significant in the collisional processes,<sup>11</sup> in our simulations computationally intensive four-body part of the potential.

To model irradiation of a nanotube lying on a heavy-atom metal substrate, we chose platinum as a substrate material since an interatomic potential was recently developed to describe the Pt-C systems.<sup>26</sup> Although gold is usually used as a nanotube substrate material, we believe that for both Pt-C and Au-C systems, the defect formation mechanism in nanotubes on such substrates is essentially the same in view of the similar behavior of collision cascades and heat spikes in these metals.<sup>27-29</sup>

The Pt-C interatomic functional form and parameter values used in our simulations are given in Appendix A; the motivation behind the potential and the results of extensive tests will be published elsewhere.<sup>26</sup> This potential reproduces well the elastic properties and melting point of Pt, and gives a comparatively weak Pt-C interaction. Thus, it can be expected to give a good picture of irradiation effects in nanotubes weakly bound to a heavy-metal substrate.

To test whether the results are sensitive to the

choice of the interatomic potential, we repeated a few simulations with an alternative parametrization (the second parametrization, see Appendix A), giving a somewhat weaker Pt-C interaction, as well as with the Brenner potential for C which includes the bond conjugation terms. For both test cases we observed only a weak nanotube-Pt interaction, slightly modifying the shape of the tube but not breaking any bonds in it. Note that the interaction between nanotubes and gold is also weak.<sup>30</sup> For both parametrizations we found no significant difference (within the statistical uncertainty) in the damage production.

To realistically model energetic collisions, we smoothly joined a repulsive potential calculated by a density-functional theory method<sup>31</sup> to the potentials for Pt and C at short interatomic separations.<sup>32</sup> The interaction between Ar and C or Pt was modelled with the Ziegler-Biersack-Littmark universal repulsive potential.<sup>33</sup>

We considered individual single-walled 100 Å-long (10,10) armchair nanotubes on Pt and graphite substrates. We also dwelled upon suspended nanotubes (free-standing nanotubes with fixed ends), but unlike our previous work,<sup>11</sup> we irradiated not only the central part but also the nanotube sides. The incidence of argon ions with energies from 100 up to 2000 eV was perpendicular to the substrate surface. The original temperature of the system was equal to zero. Open boundary conditions were used and the boundary atoms were kept fixed during the simulation time. To prevent spurious reflection of pressure waves from the borders of the system, the Berendsen temperature control<sup>34</sup> was used at the borders for the first 20 ps after ion impact, then the temperature was everywhere scaled down to zero at a rate of 1 K/ps. For every energy considered, we carried out 100 independent runs and averaged the results.

This theoretical set-up can be juxtaposed with experimental one for the low-temperature (e.g., liquid nitrogen temperature) and low-dose (less than  $10^{11}$  ion/cm<sup>-2</sup>) ion irradiation of nanotubes. The calculated damage can be related to that measured immediately after ion impact without elevating the temperature. However, carrying out such experiments at low temperatures is a challenging task. Simpler room temperature experiments will inevitably result in the annealing of at least the most unstable defects, though during a macroscopic time interval, as experiments on electron irradiation of nanotubes indicate.<sup>1,2</sup>

In order to simulate the defect annealing, we heated the system up to high temperatures (1500 K) with a subsequent quench to the zero temperature. Since macroscopic time scales are unattainable for present-day molecular dynamics simulations, we modelled the evolution of defects for 100 ps, but at elevated (1500 K) temperature. This temperature, which is lower than the Pt melting point (1900 K), made it possible to overcome the potential barriers between metastable energy configurations and gain insight into the behavior

of defects on macroscopic time scales. Several 1-ns-long control runs gave essentially the same results.

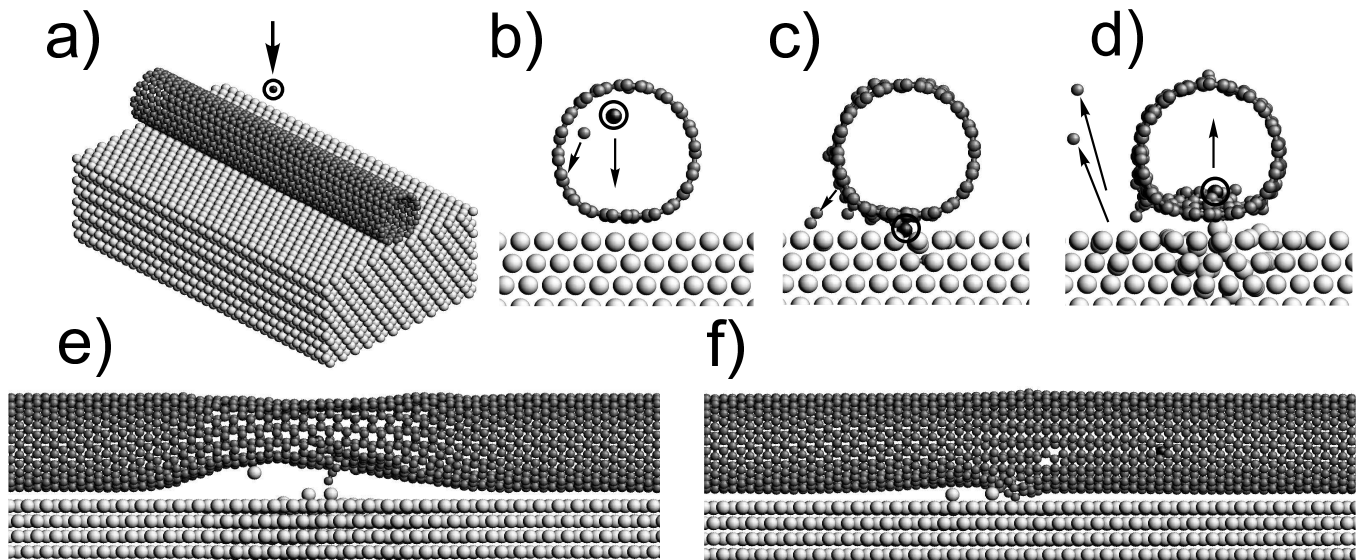


FIG. 1. Illustration of the production of defects in carbon nanotubes on Pt substrates. The initial movement direction of the impinging Ar ion (circled) is designated by the arrow. The light spheres represent Pt atoms and the darker ones C atoms. The first snapshot (a) shows the original atom configuration in the nanotube-Pt substrate system. The Ar ion creates vacancies in the uppermost part of the nanotube wall as well as primary C recoils (b). Some other C atoms are sputtered from the nanotube; the Ar ion hits the substrates and gives rise to the development of a collision cascade (c). The Ar ion is reflected back from the surface creating some extra damage in the nanotube (d). A pressure wave has developed in the nanotube (e). The final configuration after cooling down the system to the zero temperature (f).

Our goal was to estimate the irradiation-induced damage in nanotubes but not in the substrates, so we were not interested in the defects created far from the substrate surface and having no effect on the nanotube. However, we carefully took into consideration the processes in the substrates which could effect the damage in nanotubes, i.e., collision cascades and thermal spikes. Thus, we used a Pt substrate consisting of 10 - 30 atom layers in the direction of the irradiation. Such a comparatively large number of layers was indispensable for realistically modelling collision cascades in metals, especially at high ion energies. This was important since sputtered metal atoms could damage the nanotube, along with the incident ions and backscattered C recoils.

On the other hand, to model graphite substrates, we used a slab composed of only four graphite layers, because the probability of recoil backscattering was small due to the low carbon atomic mass and the large separation and weak interaction between graphite layers.

### III. RESULTS AND ANALYSIS

We start with the irradiation of nanotubes lying on the Pt substrate. Having optimized the geometry of the nanotube-substrate system by minimizing its energy, we irradiated the nanotube with argon ions as described above. The optimization resulted in the partial distortion of the *pristine* carbon network (i.e., without dangling bonds) when the first parametrization of the Pt-C potential was used. We did not observe formations of any substrate-nanotube bonds for intact carbon nanotubes. For the second parametrization we did not find any bonds either, though it resulted in more apparent deformation (flattening) of the nanotube wall near the nanotube-Pt substrate interface.

A typical illustration of the defect production mechanism upon Ar ion impact is presented in Fig. 1 where a number of snapshots corresponding to different time moments are given. The first snapshot Fig. 1(a) shows the original geometry before the impact. The motion direction of the impinging 500-eV Ar ion (circled) is designated by the arrow. The Ar ion usually creates a single vacancy (or multi-atom vacancy) in the uppermost part of the nanotube wall as well as primary carbon recoils, Fig. 1(b). Then the recoils and Ar ion produce defects in the lower part of the nanotube, Fig. 1(c), resulting in sputtering C atoms from the nanotube and producing a collision cascade in the substrate. A part of the recoils (or the Ar ion) is reflected back from the surface producing some extra damage in the nanotube Fig. 1(d). The characteristic time of these processes is about 0.1 ps. The ion impact and the sputtered substrate atoms also result in the development of a pressure wave in the nanotube Fig. 1(e) propagating to

its ends from the impact point. The oscillations in the nanotube diminishes during much longer time scale (the actual time is governed by the cooling rate). The final configuration after the system has been cooled down to the zero temperature is presented in Fig. 1(f).

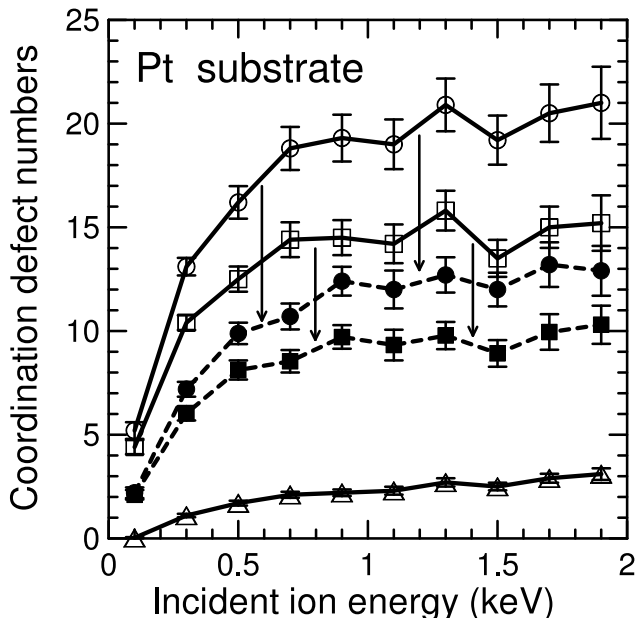


FIG. 2. Average coordination defect numbers for a nanotube lying on Pt substrate as a function of incident Ar ion energy. Open/full circles stand for the number of C atoms with a coordination other than three before/after annealing (the overall damage), open/full squares for the number of two-coordinated atoms before/after annealing. Triangles correspond to the number of sputtered C atoms. The arrows visualize the relationship between the curves before and after annealing

Visual analysis of the final atom positions indicated that, analogously to the case of suspended nanotube irradiation,<sup>11</sup> single vacancies (and vacancy-related defects<sup>5</sup> which single vacancies can turn into) are the most prolific defects in nanotubes which appear after ion impact. Two-coordinated single adatoms on both external and internal sides of the nanotube walls<sup>32</sup> were also common. Besides this, other complex defects were observed. Those were Stone-Wales defects<sup>35</sup> associated with a 90-degree-rotation of a bond in the nanotube atom network, small amorphous regions, local distortions in the network due to incorporated Pt atoms, non-hexagonal rings, and even at times very peculiar defect configurations like C-atom chains formed inside the nanotube when displaced C atoms were left in the nanotube interior.

In order to quantitatively characterize the damage in the nanotube at different energies of incident Ar ions, in Fig. 2 we plot the number of C atoms with a coordination other than three as a function of ion energy (open circles) and the number of sputtered C atoms (triangles). The former quantity may be considered as a characteristic of

the overall damage in the nanotube produced by an ion.

We also present in Fig. 2 the number of two-coordinated atoms (open squares). This quantity divided by three roughly gives the number of atoms in vacancies and vacancy-related defects in the system. For example, an ideal single vacancy in the graphene network corresponds to three two-coordinated atoms. This relation between two-coordinated atoms and vacancy atoms is qualitatively correct even for complex defects. Although a double vacancy (whose formation is frequently accompanied by the creation of two adatoms on the nanotube wall) gives only four two-coordinated atoms, the adatoms are usually two-coordinated atoms as well, so that there are six two-coordinated atoms in the system. Thus, this rule of thumb may be used for rough estimate of the number of vacancies.

A small fraction of atoms were four-coordinated, i.e., we observed formations of  $sp^3$  bonds in locally amorphized regions of the nanotube. The number of one-coordinated atoms was negligibly small since such configurations are energetically unfavorable and C atoms tend to form at least two chemical bonds with other C atoms.

It can be seen from Fig. 2 that, if the energy of the incident ion is higher than the defect creation threshold energy (about 50 eV, see Ref. 11), the number of defects increases with the energy up to roughly 600 eV, then it remains practically constant. The reason for such behavior is that at low energies the damage production grows with energy, since there is more energy available for it. At higher ion energies, although defect production in the nanotube drops as the nuclear collision cross section decreases,<sup>11</sup> there are more reflected C recoils and Pt atoms sputtered from the substrate, all of which damage the nanotube. At very high energies (several keV), the ion penetrates into the substrate rather deep, which results in the drop in the sputtering yield and, respectively, in the nanotube damage due to this mechanism. The decrease in damage due to the diminution in the cross section and the damage enhancement due to the sputtered atoms approximately counterbalance each other at energies higher than 1 keV.

The annealing of defects (as described above) gave rise to a substantial drop in the defect numbers. In Fig. 2 we also present the overall damage as a function of ion energy (full circles) as well as the number of two-coordinated atoms (full squares) after annealing. The number of sputtered C atoms (triangles) remained, of course, the same. Although about 40% of defects annealed, a substantial amount of defects remained in the system. The ratio of annealed defects can be larger at longer time-scales, but total annealing of defects is not possible since a number of atoms were sputtered from the nanotube.

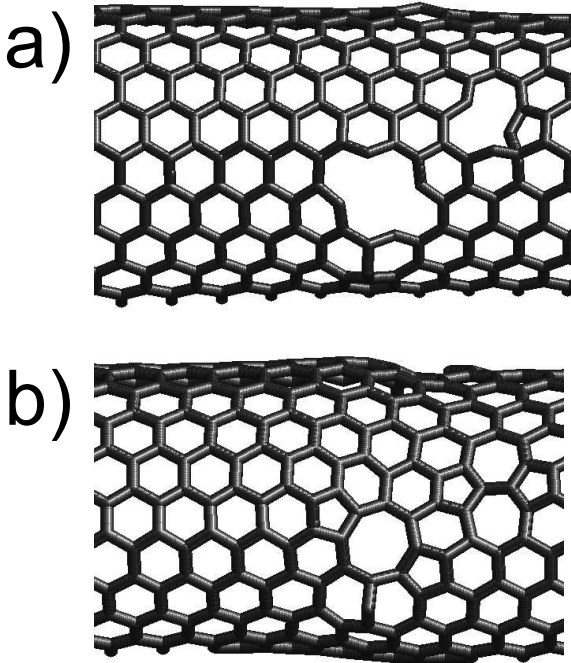


FIG. 3. Front walls of one and the same nanotube just after ion impact (a) and after annealing (b). During annealing the double vacancy in the middle of the carbon network transformed to an agglomeration of non-hexagonal rings. The single vacancy and the nearby C adatom in the upper right-hand corner of the network transformed to a Stone-Wales defect. It is also noticeable that the annealing led to local diameter reduction.

We found that two mechanisms give rise to defect annealing. The first mechanism is the recombination of vacancies and C adatoms on the nanotube walls. Note that the latter defects may be interpreted as interstitial-like defects in single-walled nanotubes,<sup>11</sup> so this recombination may be understood as the recombination of Frankel pairs. Although the mobility of such adatoms and vacancies in nanotubes is rather low (several orders of magnitude lower than that for the interstitial in graphite; a detailed study of this issue is beyond the scope of this work), our simulations provide evidence that such recombination may occur on a macroscopic time-scale at room temperature, especially given that an adatom and a vacancy are usually formed after ion impact at a distance of several Å from each other.

The second mechanism of the radiation defect annealing was the mending of vacancies through dangling bond saturation and by forming non-hexagonal rings and Stone-Wales defects. An illustration of this mechanism is given in Fig. 3 where the front walls of one and the same nanotube just after ion impact (a) and after annealing (b) are shown. It is seen that during annealing the double vacancy in the middle of the carbon network has been

transformed to an agglomeration of non-hexagonal rings. The annealing also gave rise to the transformation of the single vacancy and the nearby C adatom in the upper right-hand corner of the network to a Stone-Wales defect (two adjacent heptagons and two pentagons). It is also noticeable that the annealing led to the local diameter reduction.

The latter mechanism is similar to that of defect annealing upon electron irradiation.<sup>5</sup> This mechanism is also relevant to transformations<sup>36</sup> of single-walled nanotubes in ropes to multi-walled nanotubes due to thermal treatment at high temperatures (2500-2700 K). We emphasize here that ion irradiation creates more severe local damage than electron irradiation, since in the former case a vacancy clusters may be easily formed by an energetic ion impact, whereas in the latter case the predominant defects are single vacancies. Thus, carbon nanotubes have surprisingly high ability to heal the damage, although the topological defects still remain in the carbon network. However, at low temperatures, defect annealing occurs during a macroscopic time<sup>11</sup> as a result of which at low temperatures some metastable defects (e.g., unreconstructed vacancies) may remain in nanotubes long enough to be experimentally detected.

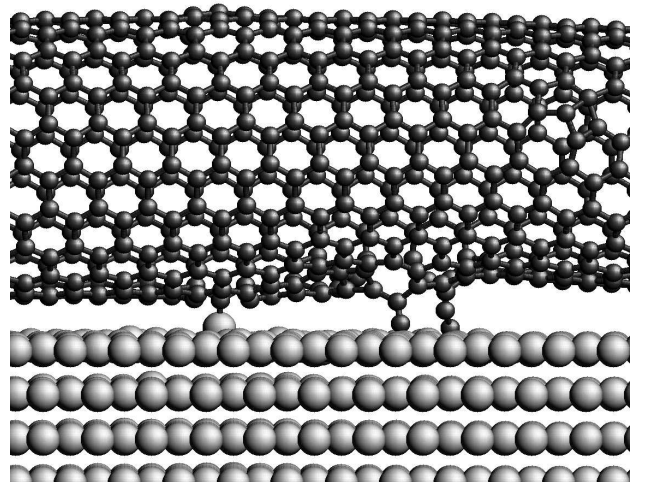


FIG. 4. Formation of bonds between a nanotube and substrate after ion impact by saturating dangling bonds near vacancies. The light spheres represent Pt atoms and the darker ones C atoms.

Another interesting effect observed in our simulations is the saturation of irradiation-induced carbon dangling bonds by forming comparatively strong bonds (typical energies of about 1 eV) between the nanotube and substrate atoms. A typical atomic configuration with such bonds (which usually appear near vacancies) is given in Fig. 4. We stress once more that we did not observe formation of any bonds between intact nanotubes and Pt substrates. Thus, the ion irradiation results in pinning the nanotube to the substrate. We also noticed that

sputtered Pt atoms sometimes got stuck on defects in nanotube walls and remain in these positions even after the annealing of nanotubes at elevated temperatures. Thus, Pt atoms may be incorporated into the carbon network if dangling bonds are present. This finding is corroborated by experiments in which Pt clusters have been observed near defects on carbon nanotube surfaces.<sup>37</sup>

Having considered nanotubes on heavy-atom metallic substrates, we now proceed to the other limiting case: nanotubes on graphite. The interaction between carbon nanotubes and graphite is very weak<sup>21,20</sup> and governed by Van der Waals forces similar to the graphite interlayer forces<sup>32</sup> or the forces between nanotubes in bundles.<sup>38</sup> Since this interaction is not essential during the collisional processes, we did not take it into account in the ion impact simulations.

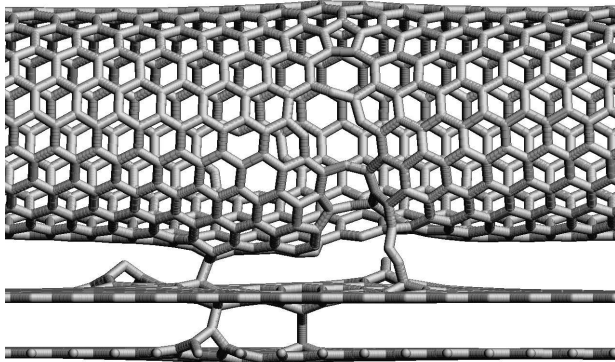


FIG. 5. Carbon nanotube-graphite interface after 700 eV ion impact which resulted in the formation of a multi-vacancy in the nanotube wall and nanotube-graphite covalent C-C bonds. Only the two uppermost graphite layers are shown.

A typical nanotube-graphite atomic configuration after a 700 eV ion impact is shown in Fig. 5. The energetic ion (which hit the nanotube side wall) resulted in the formation of a large vacancy and nanotube-graphite covalent C-C bonds. Thus, analogously to the case of Pt substrate, the ion irradiation results in the pinning of carbon nanotubes to graphite.

The number of irradiation-induced coordination defects in the nanotube on graphite is presented in Fig. 6 for different energies of the incident ions. As in Fig. 2 for Pt substrate, open circles correspond to the number of C atoms with a coordination other than three (the total damage), open squares stand for the number of two-coordinated atoms, and triangles for sputtered atoms. The defect numbers grow with the energy up to roughly 600 eV, then they remain practically constant. Note that the total damage and the number of two-coordinated atoms are lower than those for the case of Pt due to the absence of atoms sputtered from the substrate and a lower probability of energetic recoil backscattering. The number of sputtered atoms is practically the same.

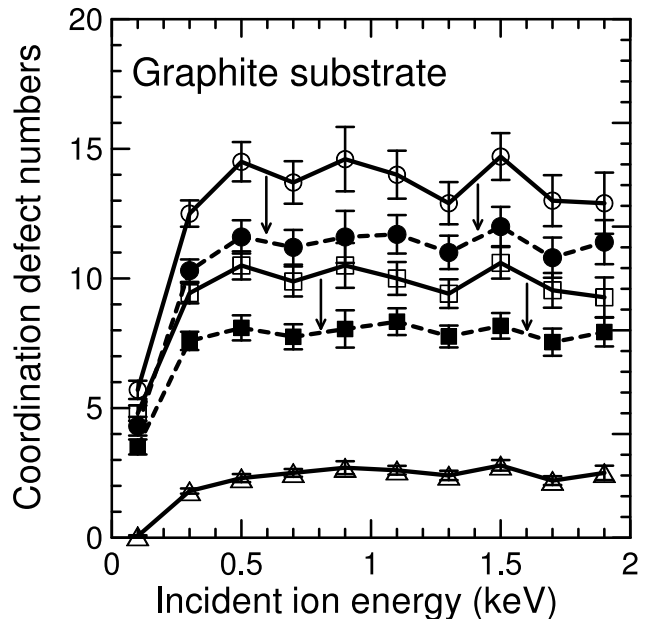


FIG. 6. Average coordination defect numbers for a nanotube lying on graphite substrate as a function of incident Ar ion energy. Open/full circles stand for the number of C atoms with a coordination other than three before/after annealing (the overall damage), open/full squares for the number of two-coordinated atoms before/after annealing. Triangles correspond to the number of sputtered C atoms. The arrows visualize the relationship between the curves before and after annealing.

As in the case of the Pt substrate, the annealing of defects also gave rise to a substantial drop in defect numbers. In Fig. 6 we present the overall damage as a function of ion energy (full circles) as well as the number of two-coordinated atoms (full squares) after annealing. The arrows connect the corresponding curves before and after the annealing. The annealing also gave rise to the formation of graphite - nanotube covalent C-C bonds in the vicinity of defects when dangling bonds originally were present either in the nanotube or the uppermost graphite sheet.

In order to gain further insight into the role of substrate in the production of defects in nanotubes under ion irradiation, in Fig. 7 we show the defect numbers calculated for irradiated suspended nanotubes before and after annealing. The numbers are very close to those obtained for nanotubes lying on graphite substrates. This result confirms the negligible role of light-atom substrates on the production of irradiation-induced defects in the supported carbon nanotubes. At the same time, it corroborates the importance of accounting for heavy-atom substrate effects if the irradiation is carried out at a low temperature.

However, as follows from our simulations, the defect coordination numbers after annealing are roughly the

same for nanotubes in all the environments considered. Although the radiation damage in nanotubes on heavy-atom substrates is much higher than that for the other cases considered, the ability of carbon nanotubes to heal the defects in the carbon network due to dangling bond saturation and adatom migration gives rise to similar amount of defects in the nanotubes after annealing. We note that for all the environments of the nanotubes, the number of sputtered C atoms (created predominantly by the first impact of the ion) was the same. It means that for nanotubes on heavy-atom substrates, the extra damage created by energetic substrate and backscattered C atoms may be annealed rather easily. This is in part due to the comparatively low energies of such atoms, which always are much less energetic than the incident ion.

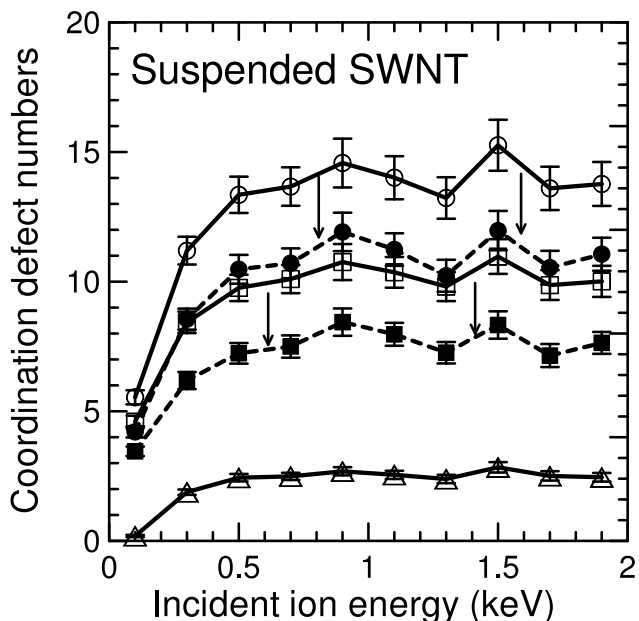


FIG. 7. Average coordination defect numbers for suspended nanotubes as a function of incident Ar ion energy. Open/full circles stand for the number of C atoms with a coordination other than three before/after annealing (the overall damage), open/full squares for the number of two-coordinated atoms before/after annealing. Triangles correspond to the number of sputtered C atoms. The arrows visualize the relationship between the curves before and after annealing.

This ability of nanotubes to mend irradiation-induced defects in the carbon network is important for using them as masks against the ion bombardment in the production of metal nanowires. Since the sputtering yield is higher for metals than that for carbon<sup>39</sup>, even single-walled nanotubes may potentially be used for making extra narrow metal wires (multi-walled nanotubes have been used in the experiments performed today<sup>10</sup>). We note, however, that further studies on the irradiation of the nanotube-substrate interface are needed to find out

what the limitations of this technique and the optimum parameters (ion energies and currents, temperature, *etc.*) are.

#### IV. SUMMARY AND CONCLUSIONS

In this paper, we examined theoretically both the irradiation of carbon nanotubes lying on different substrates and the behavior of irradiation-induced defects under annealing. We simulated the irradiation of such supported single-walled nanotubes with 100–2000 eV Ar ions using empirical potential molecular dynamics. Two different types of substrates were considered: a heavy-atom metallic substrate (platinum) and a light-atom semiconductor substrate with covalent bonds between atoms (graphite). Since macroscopic time scales are unattainable for the present-day state-of-the-art of molecular dynamics simulations, we studied the evolution of defects at room temperature by simulating the evolution of defects at elevated temperatures.

We showed that at low temperatures the defect production depends on the type of the substrate and the damage is higher for metallic substrates composed of heavy atoms due to sputtered substrate atoms and backscattered carbon recoils. The most prolific defects which appear upon irradiation are single- and multi-atom vacancies. The number of defects increases with the energy of incident ions (up to roughly 600 eV) then it remains practically the same because of a decrease in the nuclear collision cross section at higher ion energies.

We further demonstrated that the nanotube carbon network has a unique ability to heal ion-induced damage due to defect migration and dangling bond saturation. Similar behavior of nanotubes under electron irradiation has been reported, but electron irradiation creates mostly single vacancies, whereas energetic ions severely damage the nanotube producing local defect regions. The residual damage in nanotubes after annealing is independent of the substrate type.

We finally predict pinning of nanotubes to both metallic and graphite substrates upon ion irradiation. This happens through the formation of chemical bonds between the nanotube and substrate atoms. Such bonds do not exist for pristine nanotubes and appear after irradiation near irradiation-induced defects.

#### ACKNOWLEDGMENTS

We would like to thank Dr. K. Albe, Dr. F. Banhart, Prof. A. Rubio and M.Sc. E. Salonen for useful scientific discussions. The research was supported by TEKES under the FFUSION2 programme, and the Academy of Finland under projects No. 44215 and 73722. Grants of computer time from the Center for Scientific Computing in Espoo, Finland are gratefully acknowledged.

<sup>1</sup> F. Banhart, Rep. Prog. Phys. **62**, 1181 (1999).

<sup>2</sup> M. Terrones, H. Terrones, F. Banhart, J.-C. Charlier, and P. M. Ajayan, Science **288**, 1226 (2000).

<sup>3</sup> M. Terrones, F. Banhart, N. Grobert, J.-C. Charlier, H. Terrones, and P. Ajayan, submitted for publication (2001).

<sup>4</sup> H. Stahl, J. Appenzeller, R. Martel, P. Avouris, and B. Lengeler, Phys. Rev. Lett. **85**, 5186 (2000).

<sup>5</sup> P. M. Ajayan, V. Ravikumar, and J.-C. Charlier, Phys. Rev. Lett. **81**, 1437 (1998).

<sup>6</sup> C.-H. Kiang, W. Goddard, R. Beyers, and D. Bethune, J. Phys. Chem **100**, 3749 (1996).

<sup>7</sup> J. P. Salvetat, J. M. Bonard, N. H. Thomson, A. J. Kulik, L. Forro, W. Benoit, and L. Zuppiroli, Appl. Phys. A: (Mater. Sci. Process.) **69**, 255 (1999).

<sup>8</sup> A. Bachtold, M. Henny, C. Terrier, C. Strunk, C. Schonenberger, J.-P. Salvetat, J.-M. Bonard, and L. Forro, Appl. Phys. Lett. **73**, 274 (1998).

<sup>9</sup> B. Ni and S. Sinnott, Phys. Rev. B **61**, 16343 (2000).

<sup>10</sup> W. S. Yun *et al.*, J. Vac. Sci. Technol. A **18**, 1329 (2000).

<sup>11</sup> A. V. Krasheninnikov, K. Nordlund, M. Sirviö, E. Salonen, and J. Keinonen, Phys. Rev. B **63**, 245405 (2001).

<sup>12</sup> J. Nygård and D. Cobden, <http://xxx.lanl.gov>, Condmat/0108020 (2001).

<sup>13</sup> E. Salonen, A. V. Krasheninnikov, and K. Nordlund, Nucl. Instr. and Meth. in Phys. Res. B (2001), submitted for publication.

<sup>14</sup> A. V. Krasheninnikov, Sol. Stat. Comm. **118**, 361 (2001).

<sup>15</sup> T. Kostyrko, M. Bartkowiak, and G. D. Mahan, Phys. Rev. B **60**, 10735 (1999).

<sup>16</sup> H. J. Choi, J. Ihm, S. Louie, and M. Cohen, Phys. Rev. Lett. **84**, 2917 (2000).

<sup>17</sup> M. P. Anantram and T. R. Govindan, Phys. Rev. B **58**, 4882 (1998).

<sup>18</sup> D. Orlikowski, H. Mehrez, J. Taylor, H. Guo, J. Wang, and C. Roland, Phys. Rev. B **63**, 155412 (2001).

<sup>19</sup> L. C. Venema, J. W. Janssen, M. R. Buitelaar, J. W. G. Wildöer, S. G. Lemay, L. P. Kouwenhoven, and C. Dekker, Phys. Rev. B **62**, 5238 (2000).

<sup>20</sup> U. Hubler, P. Jess, H. P. Lang, H.-J. Güntherodt, J.-P. Salvetat, and L. Forró, Carbon **36**, 697 (1998).

<sup>21</sup> S. Paulson, A. Helsen, M. Nardelli, R. Taylor, M. Falvo, R. Superfine, and S. Washburn, Science **1742**, 1742 (2000).

<sup>22</sup> M. P. Allen and D. J. Tildesley, *Computer Simulation of Liquids* (Oxford University Press, Oxford, England, 1989).

<sup>23</sup> D. W. Brenner, Phys. Rev. B **42**, 9458 (1990).

<sup>24</sup> Y. Xia, Y. Ma, Y. Xing, Y. Mu, C. Tan, and L. Me, Phys. Rev. B **61**, 11088 (2000).

<sup>25</sup> M. B. Nardelli, B. I. Yakobson, and J. Bernholc, Phys. Rev. B **57**, 4277 (1998).

<sup>26</sup> K. Albe, K. Nordlund, and R. S. Averback, , submitted for publication.

<sup>27</sup> K. Nordlund, M. Ghaly, R. S. Averback, M. Caturla, T. Diaz de la Rubia, and J. Tarus, Phys. Rev. B **57**, 7556 (1998).

<sup>28</sup> M. Ghaly, K. Nordlund, and R. S. Averback, Phil. Mag. A

**79**, 795 (1999).

<sup>29</sup> K. Nordlund, L. Wei, Y. Zhong, and R. S. Averback, Phys. Rev. B **57**, 13965 (1998).

<sup>30</sup> E. Mizoguti, F. Nihey, M. Yudasaka, S. Iijima, T. Ichihashi, and K. Nakamura, Chem. Phys. Lett. **321**, 297 (2000).

<sup>31</sup> K. Nordlund, N. Runeberg, and D. Sundholm, Nucl. Instr. Meth. Phys. Res. B **132**, 45 (1997).

<sup>32</sup> K. Nordlund, J. Keinonen, and T. Mattila, Phys. Rev. Lett. **77**, 699 (1996).

<sup>33</sup> J. F. Ziegler, J. P. Biersack, and U. Littmark, *The Stopping and Range of Ions in Matter* (Pergamon, New York, 1985).

<sup>34</sup> H. J. C. Berendsen, J. P. M. Postma, W. F. van Gunsteren, A. DiNola, and J. R. Haak, J. Chem. Phys. **81**, 3684 (1984).

<sup>35</sup> A. Stone and D. Wales, Chem. Phys. Lett. **128**, 501 (1986).

<sup>36</sup> M. J. López, A. Rubio, J. A. Alonso, S. Lefrant, K. Méténier, and S. Bonnamy, (2001), submitted for publication.

<sup>37</sup> B. C. Satishkumar, E. M. Vogl, A. Govindaraj, and C. N. R. Rao, J. Phys. D: Appl. Phys **29**, 3173 (1996).

<sup>38</sup> M. J. López, A. Rubio, J. A. Alonso, L.-C. Qin, and S. Iijima, Phys. Rev. Lett. **86**, 3056 (2001).

<sup>39</sup> R. Berish, *Sputtering by Particle Bombardment* (Springer, Berlin, 1981).

## APPENDIX A: INTERATOMIC POTENTIAL PARAMETERS

The parameters of the C-C potential employed in our simulations are given in Ref. 23. Since an extensive description of the principles used in the C-Pt and Pt-Pt potential development is presented in Ref. 26 we list only the parameter values here.

The potential energy is written as a sum over individual bond strengths:

$$V_{Eq} = \sum_{i>j} f_{ij}(r_{ij}) \left[ V_{ij}^R(r_{ij}) - \frac{B_{ij} + B_{ji}}{2} V_{ij}^A(r_{ij}) \right]. \quad (\text{A1})$$

$$V^R(r) = \frac{D_e}{S-1} \exp\left(-\beta\sqrt{2S}(r-R_e)\right),$$

$$V^A(r) = \frac{SD_e}{S-1} \exp\left(-\beta\sqrt{2/S}(r-R_e)\right), \quad (\text{A2})$$

The cutoff function  $f_{ij}$  is used to restrict the interaction to the next neighbors and is defined as:

$$f(r) = \begin{cases} 1, & r \leq R_{\text{cut}} - D_{\text{cut}}, \\ \frac{1}{2} - \frac{1}{2} \sin\{\pi(r - R_{\text{cut}})/(2D_{\text{cut}})\}, & |R_{\text{cut}} - r| \leq D_{\text{cut}}, \\ 0, & r \geq R_{\text{cut}} + D_{\text{cut}}, \end{cases} \quad (\text{A3})$$

with  $D_{\text{cut}}$  and  $R_{\text{cut}}$  as adjustable parameters. The many-body term is adopted from Brenner<sup>23</sup> and is formulated as:

$$B_{ij} = (1 + \chi_{ij})^{-1/2},$$

$$\chi_{ij} = \sum_{k(\neq i,j)} f_{ik}(r_{ik}) g_{ik}(\theta_{ijk}) \exp[2\mu_{ik}(r_{ij} - r_{ik})], \quad (\text{A4})$$

$$g(\theta_{ijk}) = \gamma \left( 1 + \frac{c^2}{d^2} - \frac{c^2}{[d^2 + (h + \cos\theta_{ijk})^2]} \right). \quad (\text{A5})$$

The parameter values used for Pt-Pt were:  $D_o=3.71$  eV,  $r_o = 2.34 \text{ \AA}$ ,  $\beta=1.65921 \text{ \AA}^{-1}$ ,  $\gamma = 0.20967626783$ ,  $S = 1.79493$ ,  $c = 0.0$ ,  $d = 1.0$ ,  $h = 1.0$ ,  $2\mu = 2.03801 \text{ \AA}^{-1}$ ,  $R_{cut} = 3.4 \text{ \AA}$ ,  $D = 0.2 \text{ \AA}$ .

The parameter values used for Pt-C were as follows.

The first parametrization:  $D_o=5.3$  eV,  $r_o = 1.84 \text{ \AA}$ ,  $\beta=1.836 \text{ \AA}^{-1}$ ,  $\gamma = 0.0097$ ,  $S = 1.1965$ ,  $c = 1.23$ ,  $d = 0.36$ ,  $h = 1.0$ ,  $2\mu = 0.0 \text{ \AA}^{-1}$ ,  $R_{cut} = 2.65 \text{ \AA}$ ,  $D = 0.15 \text{ \AA}$ .

The second parametrization:  $D_o=5.3$  eV,  $r_o = 1.813 \text{ \AA}$ ,  $\beta=1.80472 \text{ \AA}^{-1}$ ,  $\gamma = 0.03129814$ ,  $S = 1.1$ ,  $c = 2.63584$ ,  $d = 1.73596$ ,  $h = 1.0$ ,  $2\mu = 0.0 \text{ \AA}^{-1}$ ,  $R_{cut} = 2.65 \text{ \AA}$ ,  $D = 0.15 \text{ \AA}$ .